Joint acoustic energy harvesting and noise suppression using deep-subwavelength acoustic device

IOP Publishing Smart Materials and Structures
Smart Mater. Struct. 29 (2020) 035012 (13pp) https://doi.org/10.1088/1361-665X/ab6697

Joint acoustic energy harvesting and noise suppression using deep-subwavelength acoustic device

Ming Yuan[1,4], Xiao Sheng[2], Ziping Cao[2,4], Zongqiang Pang[1] and Guoliang Huang[3,4]

[1] School of Automation, Nanjing University of Posts and Telecommunications, 210023 Nanjing, People's Republic of China
[2] School of Telecommunications and Information Engineering, Nanjing University of Posts and Telecommunications, 210023 Nanjing, People's Republic of China
[3] Department of Mechanical and Aerospace Engineering, University of Missouri, Columbia, MO 65211, United States of America

E-mail: yuanming@njupt.edu.cn, caozp@njupt.edu.cn and huangg@missouri.edu

Received 5 September 2019, revised 15 November 2019
Accepted for publication 31 December 2019
Published 29 January 2020

Abstract

Aiming to simultaneously realize acoustic energy harvesting (AEH) and noise suppression, this study proposes a novel deep subwavelength acoustic device. The proposed device is composed of an acoustic resonator with a compliant bottom. At the acoustic resonance frequency of the device, sound pressure difference will excite the compliant part and generate substantial strain energy within the substrate. The electrical energy is then generated from the bonded piezoelectric patch on the substrate. Specifically, an embedded logarithmic spiral neck is adopted to make the device compact. Moreover, compared to the uniform neck configuration, the proposed spiral configuration is able to improve sound pressure amplification performance, which is demonstrated via numerical simulation and experimental studies. For the single AEH unit performance, experimental results show 8.1 μW electrical power can be harvested at 100 dB sound pressure level (SPL) excitation. At the acoustic resonant frequency, the proposed device is deep subwavelength, which is only 1/76 of the interested wavelength. Furthermore, when the AEH array configuration is adopted, simultaneous noise and energy harvesting functions can be realized. Experimental results show that the acoustic energy can be converted into electrical power, which is able to power a pedometer device. Meanwhile, the noise reduction performances concerning different excitation cases are notable. The proposed AEH system saves space and is multifunctional, which can be applied to the industrial application in the near future.

Keywords: acoustic energy harvesting, deep-subwavelength acoustic device, low frequency noise, noise suppression

(Some figures may appear in colour only in the online journal)

1. Introduction

The internet of things (IoT) helps in making devices smarter, allowing devices to be able to realize one or multiple functions related to sensing, triggering, communication, and control. These autotomized or supervised actions require electrical energy, but the distributed nature and low power consumption properties of IoT make the energy supply different from the classical power supply via grid [1–3].

Frequently, the IoT devices are powered with the help of chemical batteries with limited capacity. If no external power supply is available, the deployed devices will be shut down when the battery is exhausted. This will increase the maintenance cost and the discarded batteries will also increase the ecological burden. To solve this issue, environmental energy harvesting technologies have become essential approaches,

[4] Authors to whom any correspondence should be addressed.

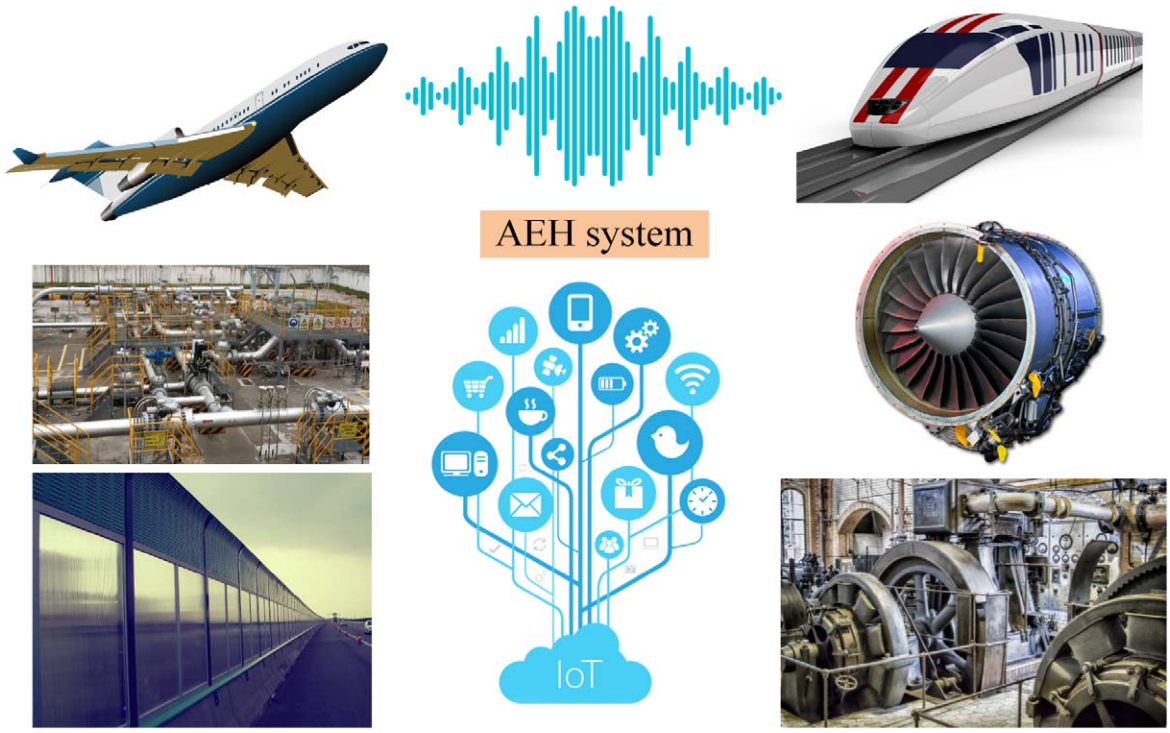

Figure 1. Potential applications of the AEH system.

converting renewable environmental energies into electrical energy for consumption by the IoT devices.

There are multiple environmental energy sources, such as wind energy, solar energy, thermal energy, and vibrational energy. Following these energy types and their specific characteristics, many efforts have been made to develop different energy harvesting technologies, where substantial advances have been achieved [4–6].

Moreover, in recent years, another environmental energy harvesting technique, referred to as acoustic energy harvesting (AEH), has increasingly attracted the interest of scientists [7–9]. The AEH technique aims to convert environmental acoustic energy into electrical energy via specially designed devices, providing electrical power to IoT devices.

As shown in figure 1, the AEH technique has potential applications for expressways, airports, acoustic liners, noise barriers, ducts, and industrial fields, where these areas share the same feature of having fluent acoustic energy [10, 11].

For the noise measurement, dBA means the sound pressure level (SPL) is weighted by A-weighting filter. Attributable to the fact that the human ear is insensitive to low frequencies, A-weighting has been widely applied in the sound level measurement to simulate the perception of the human ear [12]. The low frequency (0–500 Hz) response curves of A-, C-, and Z-weighting filters are presented in figure 2.

According to figure 2, the A-weighting filter remarkably suppresses sound signals in the low frequency range. This signifies that, when the measurement is carried out through the A-weighting in the low frequency, the physical sound pressure is much larger than the perception of human beings.

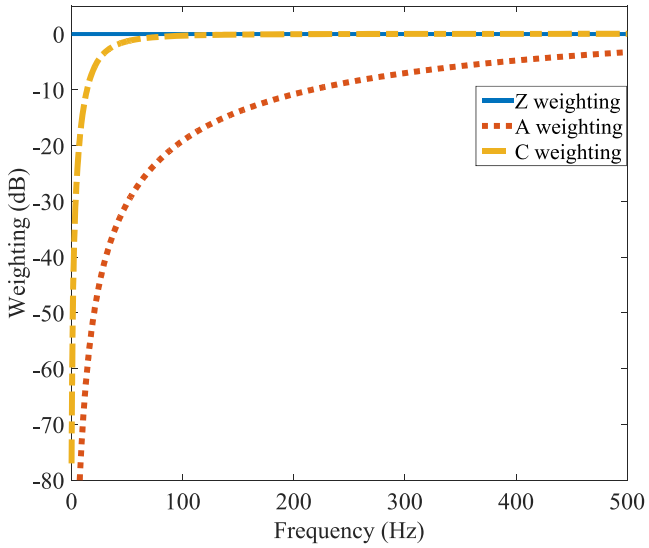

Figure 2. Frequency response curves of different weighting filters.

In further step, if the noise spectrum is examined from the commonly seen noise sources, the low frequency noise will usually occupy the dominant role in the measured spectrum, which has apparent harmonic characteristics [13–16]. Usually, the harmonic components are closely linked to the blade pass frequency or the electrical excitation frequency of the rotor. Meanwhile, the noise sources contribute to structural acoustics, making the equipped plate structure adequately excited, and efficiently radiates in the low frequency range [17]. In addition, noise can be hardly absorbed or insulated in the low frequency band, which propagates across long distances.

These above low frequency noise characteristics indicate that the low frequency acoustic waves can be utilized as an energy source, and electrical energy can be obtained with a proper energy conversion mechanism.

Owing to the fact that the sound wave excitation is weak, a specially designed structure is often applied to augment the sound pressure. To transform the acoustic energy into electrical energy, piezoelectric, electromagnetic, and triboelectric approaches can then be employed.

In previous studies, the Helmholtz acoustic resonator is adopted to amplify the incident sound pressure [18–24], as well as the fluid ripple pressure [25, 26]. The quarter-wavelength acoustic resonator has also been investigated, revealing that substantial electrical power can be generated [27]. However, these two configurations suffer from large bulk size and high fabrication cost in the low frequency range [28], hindering the deployment and application of the AEH system. Therefore, the development of a deep subwavelength AEH device is pressing in the interested low frequency range.

Recently, the development of metamaterial structures further inspired the development of AEH [29–34], which helps the AEH device become more compact and efficient. For instance, Wang proposed layered acoustic metamaterial to increase the output voltage level and realize AEH at 318 Hz with the optimal load condition [35]. Yuan proposed a helix structure to realize low frequency AEH at 175 Hz [36]. Nguyen obtained the best design in terms of AEH harvesting efficiency in low-frequency noise (198 Hz) through a numerical study [37]. Sun proposed a coiled acoustic metamaterial structure to confine the sound energy and realize AEH at 600 Hz [38]. Qi utilized acoustic multilateral metasurfaces and a piezoelectric bimorph to realize AEH at 3430 Hz [39]. An ultrathin planar metasurface-based AEH device was proposed, which exhibits a flat shape and advantages in mechanical rigidity [40]. Recently, the AEH device has been demonstrated in an airport for practical demonstrations, which can realize broadband AEH capability [41].

Meanwhile, the AEH device is anticipated to be multifunctional, and joint AEH and noise suppression are anticipated in nature, which are analogous to the simultaneous vibrational energy harvesting and structure vibration suppression [42–45].

However, the investigations of joint AEH and noise suppression investigation are still insufficient. For limited cases, an acoustic metasurface with hybrid resonances was proposed, which can realize perfect sound absorption and excellent acoustic-electrical energy conversion [46]. Pre-stressed local resonant metamaterial was proposed, which can realize more than 20 dB sound transmission loss while maintaining the acoustical-electrical ability at 432 Hz [47]. A Helmholtz resonator with a built-in decorated membrane has a maximum power output at 453 Hz and prohibits noise transmission around 364 and 453 Hz [48]. A metawall noise barrier was proposed to harvest the incident noise. Simulation results revealed that the AEH performance is promising, though the experimental work is still being undertaken [49].

According to these previous findings, most of the research focuses on the performance of one single AEH unit, while the AEH array, which is essential for the AEH engineering application, is being given less attention. Additionally, previous studies disable air ventilation to simultaneously realize noise reduction and AEH. However, this is not feasible for the duct noise application since it requires air ventilation. Finally, the power supply of AEH to a realistic electronic device has not been shown, and the harvested power value is usually obtained under the impedance matching condition via a resistance box.

In this study, a novel deep-subwavelength acoustic device that can be deployed into array and simultaneously realize AEH and noise suppression is proposed. In section 2, the construction of the proposed AEH device is illustrated. In section 3, modeling and numerical simulations are conducted, demonstrating the advantages of the proposed structure. In section 4, the acoustic properties and AEH performance of a single unit are investigated via experimental study. In section 5, the proposed AEH units are assembled into array form, which is mounted on a duct. The experimental findings are presented to demonstrate the performances of AEH and noise reduction.

2. Proposed deep-subwavelength AEH device

The schematic diagram of the proposed deep-subwavelength device is presented in figure 3. At one side of the incident cap, an acoustic inlet enables the external air fluid to enter into a spiral neck, which is bonded onto the cap and aligned to the acoustic inlet. This spiral neck configuration forms a sound passage path within the structure. The opening outlet of the neck is linked to a sound cavity, which is formed by a cylinder. At the end of the cylinder, a metallic substrate is bonded with the cylinder, serving as the back panel. A piezoelectric patch is attached at the center of the metallic substrate.

In the proposed structure, the thickness of the cap and cylinder wall is 2 mm, the height of the internal cylinder is 30 mm, and the internal radius of cylinder is 38 mm. The ratio of piezoelectric patch diameter and metallic substrate has a preferred range to generate sufficient electric charge and avoid charge cancellation. According to the previous findings [50, 51], the optimum radio is between 0.42 and 0.707. For the case presented in the present study, the radius ratio is 0.46.

The radius of acoustic inlet is 5 mm and the average length of the spiral neck is 115 mm.

Compared to the classical Helmholtz resonator, which is shown in figure 4, three major differences should be mentioned for the proposed structure. Firstly, the extended straight neck of classical Helmholtz resonator is modified into a spiral form, which can be embedded within the sound

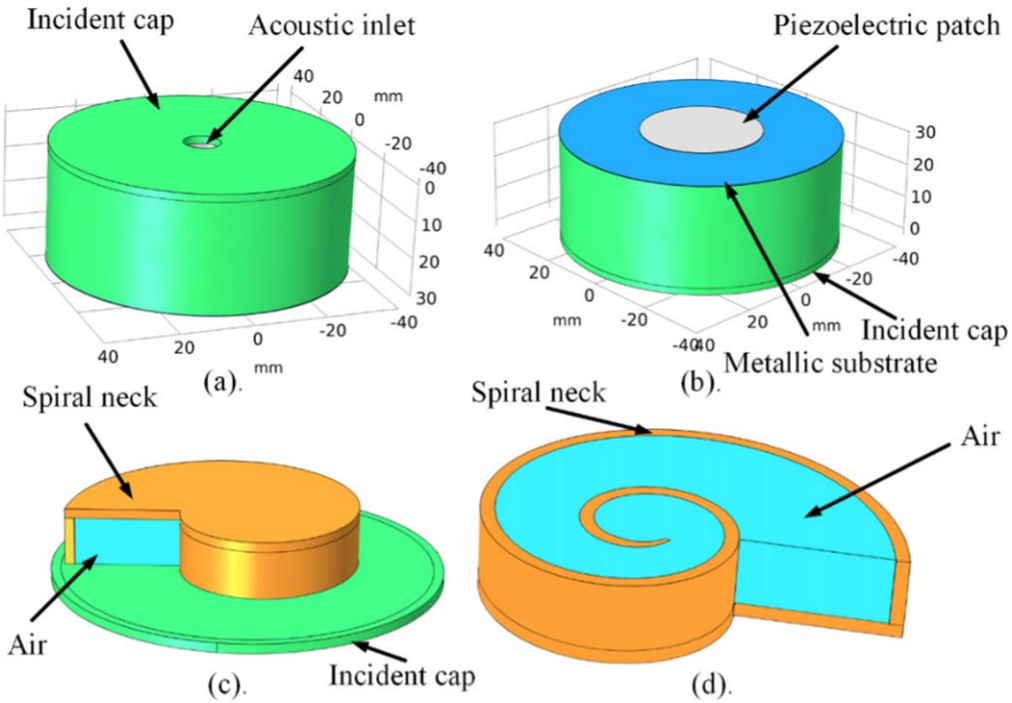

Figure 3. Schematic diagram of the proposed device. (a) Structure view from the incident side. (b) Structure view from the other side. (c) Spiral neck is bonded to the cap. (d) Spiral configuration of the neck.

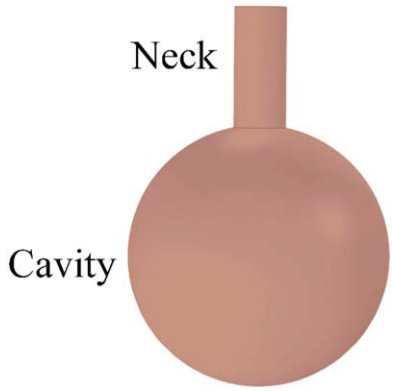

Figure 4. Schematic diagram of the classical Helmholtz resonator.

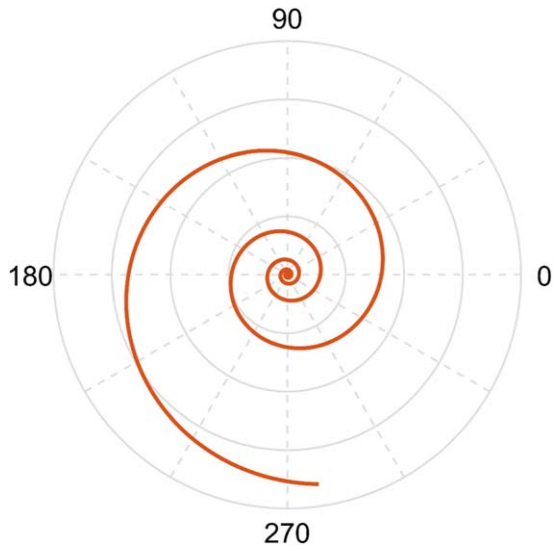

Figure 5. Schematic diagram of logarithmic spiral.

cavity. Secondly, the back panel of the cavity becomes flexible rather than rigid. Finally, the cross sectional area of the neck gradually increases (from 78.5 to 214.4 mm^2) rather than remaining as a fixed number.

Interestingly enough, the logarithmic spiral can be found in a number of diverse places, such as from the nautilus shell to galaxy formations. In polar coordinates (r, θ), the distance of this kind of spiral obeys the accompanying law, which can be written as follows:

$$r = ae^{b\theta}. \tag{1}$$

The schematic diagram of this kind of spiral ($a = 0.0013$, $b = 0.1667$, final $\theta = 19.55\pi$) is presented in figure 5.

As the curve grows, the distance between the successive turns increases. When the logarithmic spiral is extruded into a 3D neck structure, its cross sectional area will be increased as a consequence. The benefits of such design will be enumerated in sections 3 and 4.

At a specific frequency, the proposed structure can generate acoustic resonance phenomenon, and the sound pressure in the cavity can be greatly amplified. This will introduce significant sound pressure differences between the

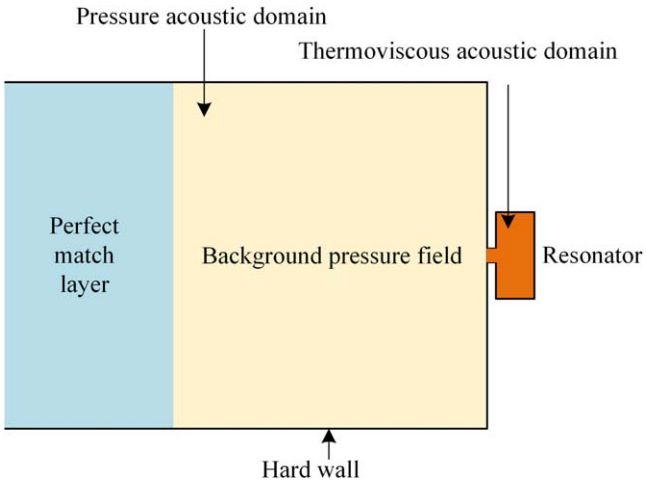

Figure 6. Schematic diagram of the numerical calculation.

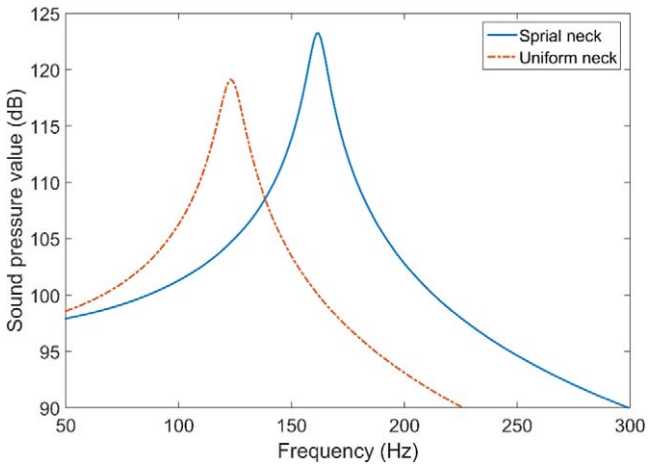

Figure 7. Sound pressure amplification comparison.

two sides of the back panel, exciting the structure. Accordingly, the strain energy is accumulated in the back panel and, owing to the piezoelectric effect, the attached piezoelectric patch converts the strain energy into electrical energy.

3. Modeling and numerical simulation

3.1. Acoustic resonator with logarithmic neck

The numerical model is built up in the COMSOL™ environment and the schematic diagram is shown in figure 6. Here, a background pressure field (1 Pa) is used to excite the proposed resonator. For simplicity and to lower the computational burden, the back panel is treated as rigid in the model. Perfect match layer is added to the background pressure field, which can absorb the reflected sound wave. Thermoviscous acoustic domain is adopted to characterize the proposed acoustic resonator, which incorporates the air fluid losses. In general, the thermoviscous effect should be considered in the narrow spaces because of the boundary layer effect. Especially when the thickness of boundary layer is relatively thick.

To make a comparison, besides the proposed structure with logarithmic neck, the acoustic resonator with uniform neck is calculated, and the obtained SPL values in the cavity are plotted in figure 7.

It is shown that the proposed acoustic structure has higher SPL gain than the acoustic resonator with uniform neck, whereas the acoustic resonant frequency occurs with a higher value. Since the sectional area of the neck becomes gradually larger, this kind of structure behaves like an acoustic horn, which is an effective approach to realize impedance transformation and increase energy flow into the cavity.

3.2. Acoustic resonator with flexible back panel

When the rigid wall at the back is changed into a flexible wall, the resonant frequency will also be changed. Here, the influence of the compliant back plate on the acoustic resonant frequency is illustrated.

To simplify the analysis, the classical Helmholtz resonator assumes that the walls are rigid and the friction losses are neglected. The air in the neck can be represented as an acoustic mass element. In addition, the air in the cavity behaves like a spring element, which can be represented as an acoustic compliance element.

When the back panel becomes flexible, it can be treated as an appended compliance for the acoustic system. The electrical analogy circuit is displayed in figure 8. The incident voltage behaves like a voltage source p_{inc} and the fluid in the neck is acoustic mass L_1, the fluid in the sound cavity is referred to as acoustic compliance C_1.

For a clamped plate, its acoustic compliance can be approximately [52]:

$$C_2 = \frac{\pi r^6 (1 - \nu^2)}{16 E h^3}, \tag{2}$$

where r is the radius of plate, ν is Poisson's ratio, E is Young's modulus, and h is the thickness of plate.

When the thickness of plate is gradually decreased, the back panel will become more flexible, and the value of C_2 becomes larger. Therefore, the total compliance value $C_T = C_1 + C_2$ is increased.

The resonant frequency occurs at the frequency under the condition:

$$f = \frac{1}{2\pi\sqrt{L_1 C_T}}. \tag{3}$$

Accordingly, when the compliance is increased, the resonant frequency will also be decreased.

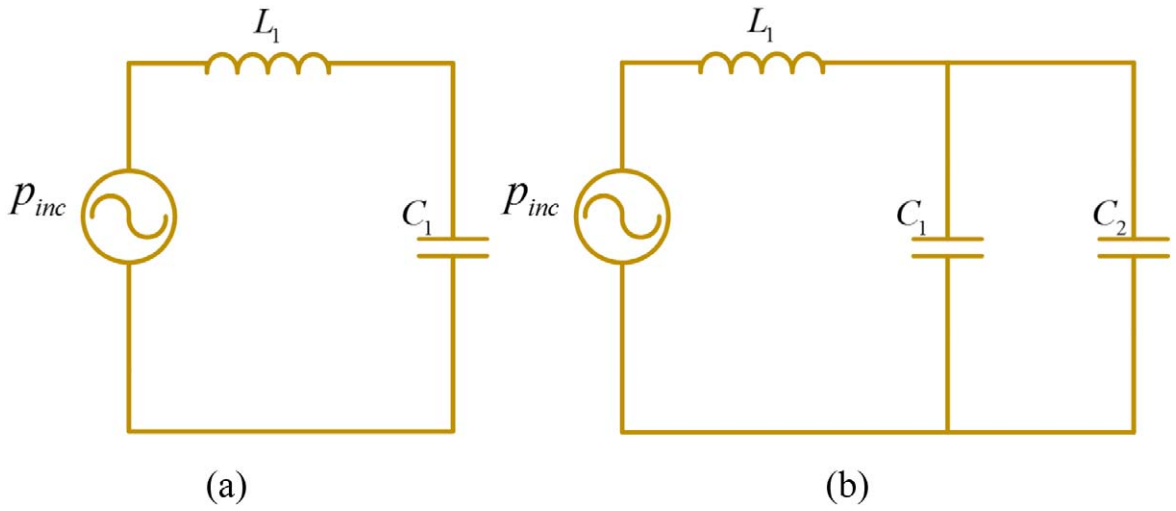

Figure 8. Acoustical-electrical analogy. (a) Classical Helmholtz resonator. (b) Modified acoustic resonator with compliant back panel.

In summary, the flexible back panel will lower the acoustic resonant frequency. This prediction agrees with the experimental results provided in section 4 and [52, 53].

4. Single AEH unit experimental investigations

4.1. AEH unit fabrication

To fabricate the proposed device, 3D printing additive manufacturing is utilized to offer the spiral neck, cylinder, and cap. A piezoelectric patch (PZT-5H) is bonded at the center of a metallic substrate (structural steel), which converts structural strain energy into electrical energy. The thickness of substrate and piezoelectric patch equals 0.2 mm, respectively. These decentralized components, which are shown in figure 9, will be bonded into an integrated AEH unit with the help of super glue.

The photograph of an AEH unit after fabrication is shown in figure 10, and the geometrical properties of the unit are provided in table 1.

4.2. Sound pressure amplification ratio

In addition to the logarithmic neck configuration, the uniform neck (formed by Archimedes spiral) configuration is fabricated for comparison to evaluate the realistic sound pressure amplification. In the AEH study, the pressure difference (AEH unit's internal pressure and ambient pressure) is essential and a larger difference value is favorable. The pressure difference serves as the excitation source to the metallic substrate and the piezoelectric patch, the acoustic energy will be converted into strain energy, then being converted into electrical energy with the help of piezoelectric effect.

Figure 11 shows the two different configurations.

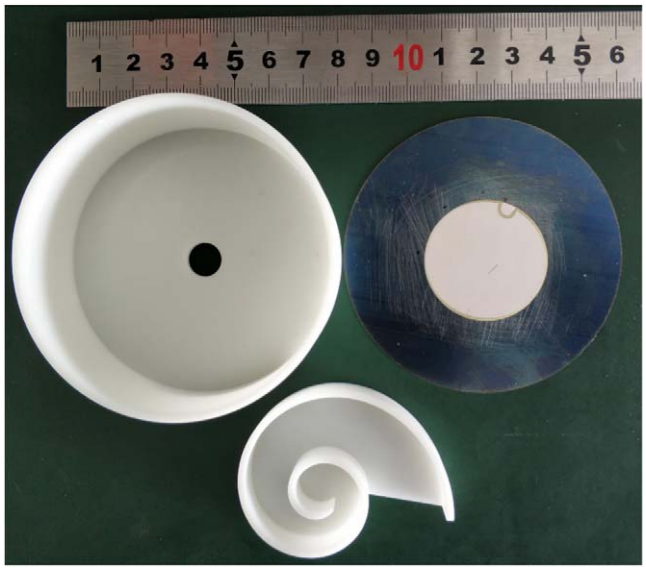

Figure 9. Photograph of the necessary components of one unit.

Three cases are considered:

Case 1. Uniform neck is mounted in the cylinder, which is covered with rigid back panel (thickness 2 mm, 3D printed cap).

Case 2. Logarithmic neck is mounted in the cylinder, which is covered with rigid back panel (thickness 2 mm, 3D printed cap).

Case 3. Logarithmic neck is mounted in the cylinder, which is covered with flexible panel (substrate 0.2 mm structural steel, PZT-5H patch 0.2 mm).

To monitor the internal sound pressure, a hole ($\Phi = 7$ mm) is built on the cylinder for microphone mounting. Two microphone sensors (G.R.A.S. 40PP) are adopted, where one is placed

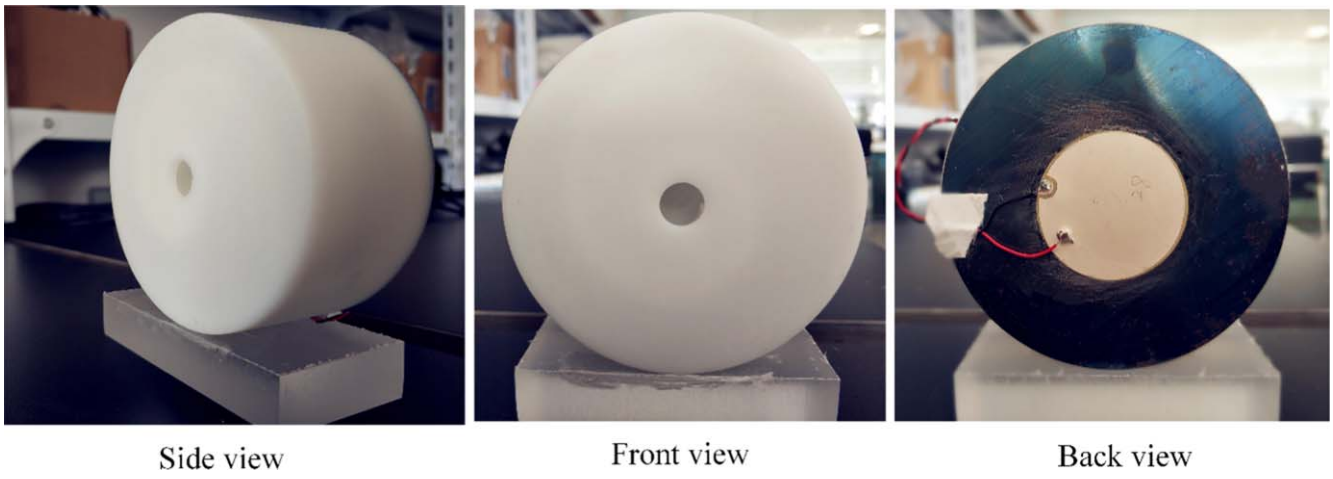

Figure 10. Photograph of the fabricated AEH sample.

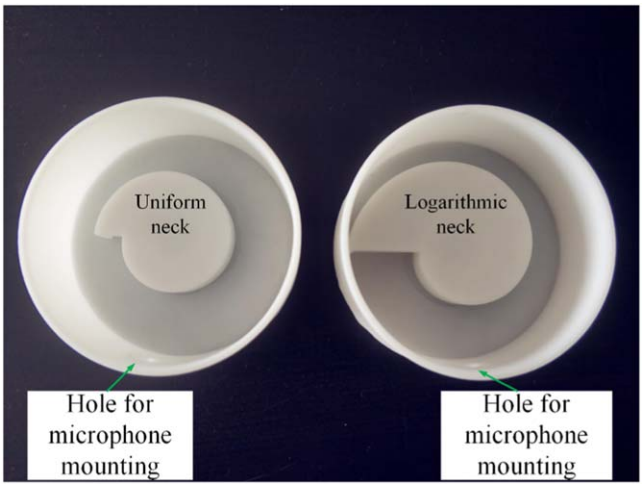

Figure 11. Test samples with different neck configurations.

Table 1. Geometrical properties of a single unit.

Parameter	Value (mm)
Height	32.4
Outer diameter	40
Wall thickness	2
Radius of inlet	5
Radius of substrate	40
Thickness of substrate	0.2
Radius of PZT patch	17.5
Thickness of PZT patch	0.2

near the incident surface and the other is placed within the cylinder.

The photograph of the experimental test is shown in figure 12.

The interesting frequency range is 100–200 Hz. A sweep sine signal is used to excite the loudspeaker and sound pressure signals from the two microphone channels, and they

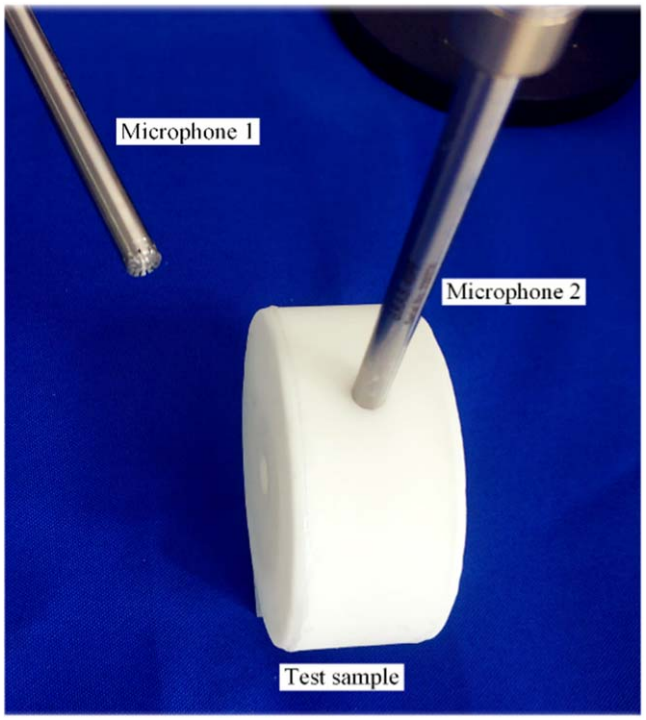

Figure 12. Sound pressure amplification ratio evaluation.

are simultaneously acquired via the PXI-4461 module. The measured results are plotted in figure 13.

Following the experimental data, the acoustic resonant frequencies are examined first. As shown in figure 13, for Cases 1 and 2, the test results show that the resonant frequencies of numerical predictions (section 3.1) are in agreement with the experimental test results (Case 1: numerical 123 Hz, experimental 120 Hz; Case 2: numerical 162 Hz, experimental 158 Hz). The resonant frequency of Case 3 is 140 Hz, which is lower than the resonant frequency of Case 2 because of the flexible bottom influence, which is in agreement with the analytical conclusions provided in section 3.2.

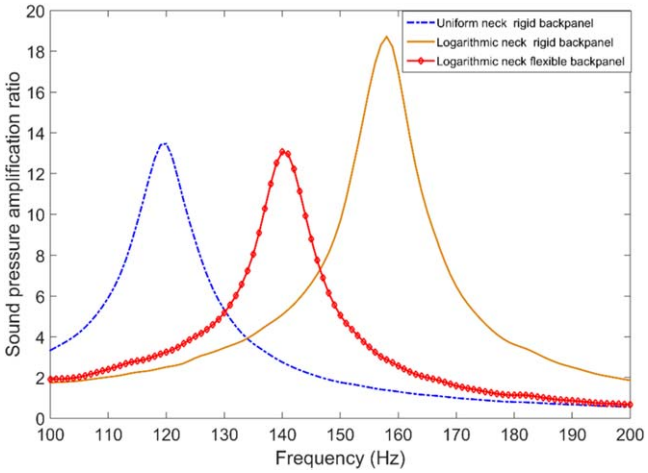

Figure 13. Sound pressure amplification ratio with different configurations.

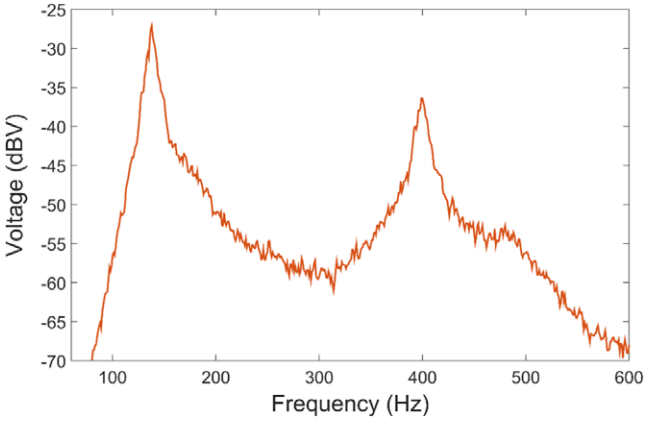

Figure 14. Voltage spectrum of the piezoelectric patch.

Secondly, the test results show that the configuration of Case 1 has a more superior sound pressure amplification performance than Case 2. The former sound pressure amplification ratio is 18.72, whereas the latter is only 13.47. The SPL value is smaller than the simulation result. One important reason for this is that in the simulation the walls are treated as perfectly rigid. However, in realistic situations, the plastic wall is not perfectly rigid, and the material damping will also lower the amplification gain [54].

Meanwhile, when the back panel is changed from rigid to flexible, the sound pressure amplification ratio of Case 3 is reduced from 18.72 (Case 2 value) to 13.07. However, the pressure amplification with flexible bottom is almost equal to that of Case 1 with rigid bottom, which demonstrates the superiority of such design.

Furthermore, the voltage signal generated from piezoelectric patch is evaluated. Band-limited white noise (50–600 Hz) is adopted to excite the fabricated sample of Case 3. The generated electrical signal is measured using PXI-4070 DMM (Digital Multi Meter) module, and the obtained voltage spectrum is shown in figure 14.

It is evident that there are two resonant peaks within the interested frequency range. The first resonant frequency corresponds to the previously mentioned acoustic resonant frequency. The second resonant frequency, which occurs at 400 Hz, corresponds to the substrate mechanical resonant frequency, which can be verified through finite element analysis.

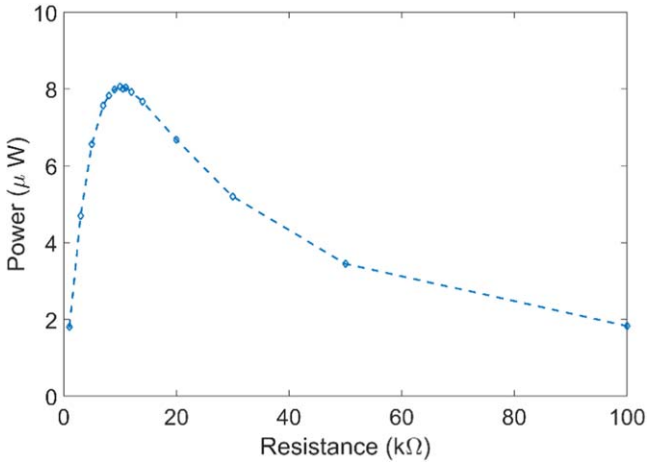

Figure 15. AEH performance of a single unit.

Owing to the strong sound excitation at acoustic resonant frequency, the measured voltage signal is 10 dB larger than the voltage signal at the mechanical resonant frequency, indicating that the proposed acoustic device is suitable for the low frequency AEH application.

4.3. Energy harvesting performance

The harvested power is evaluated under 140 Hz, 100 dB SPL (zero weighting) excitation. Attributable to the fact that the maximum power is achieved under the impedance matching condition, a decade box is linked to the piezoelectric patch, which can alter the external load resistance value.The harvested power is calculated according to the equation:

$$P = V_{PP}^2/8R, \tag{4}$$

where V_{PP} is peak-peak voltage and R is the external resistance value. The measured power with different external resistance is shown in figure 15.

Therefore, the harvested power can reach up to 8.1 μW, which is obtained when the impedance is equal to 10.5 kΩ.

At the interested frequency 140 Hz, the acoustic wavelength is 2.45 m. With respect to the proposed device, the total height is 0.0322 m, which is only 1/76 of the interested wavelength. Therefore, the proposed AEH structure is deep subwavelength.

5. AEH array experimental investigations

5.1. AEH array fabrication and energy harvesting performance

As shown in section 4, one AEH unit can generate 8.1 μW under 100 dB SPL excitation. When the excitation strength is increased, the harvested power will be increased as a consequence. For instance, the output power can be up to

Figure 16. Fabrication of AEH array with four units.

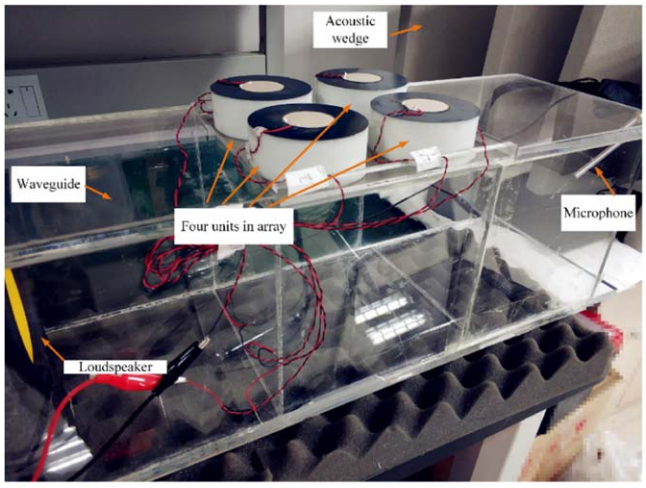

Figure 17. Experimental system for AEH array study.

200 μW when the excitation strength is increased to 114 dB. However, it should be noted that, for most circumstances, high level SPL excitation is rare. Therefore, to increase the output power of the AEH device, a practical solution is to adopt the AEH array configuration, which contains multiple AEH units.

According to the design of the present study, the proposed units can be easily assembled into an AEH array. To fulfill this task, a large aluminum plate will replace incident cap of the units. The thickness of the wall is 2 mm and circular holes (radius 5 mm) are manufactured through the plate using CNC (Computer Numerical Control) machines. The 3D printed necks are then bonded to the aluminum plate, which is shown in figure 16. Meanwhile, the cylinders are bonded to

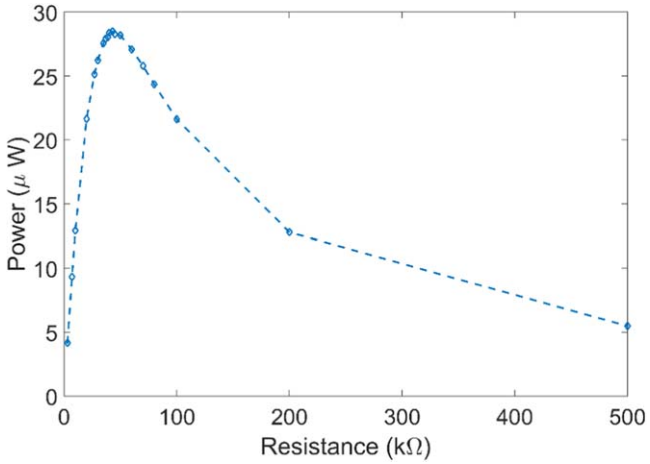

Figure 18. AEH performance of four units in array and electric circuit linked in series.

the aluminum plate. Finally, the metallic substrates (with piezoelectric patch) are bonded to the cylinder.

Since the acoustic resonant state occurs within each AEH unit, the coupling between the units can be neglected, making the resonant frequency a constant value. This decoupling property is very important for the AEH array deployment. The strong charge cancellation will not occur if multiple units are wired in series or in parallel, and the interface circuit can be simplified.

To demonstrate the practical AEH array application, a waveguide was fabricated with a thickness of 10 mm acrylic material. The inner cross-sectional dimension of the waveguide is 175 mm $\times$ 175 mm. A five-inch loudspeaker is mounted at one side of the waveguide and the fabricated array is mounted at the middle part of the waveguide. At the open end of the waveguide, one 1/4 inch microphone sensor (G.R. A.S. 40PP) is utilized to monitor the sound pressure variation. The photograph of the experimental system is shown in figure 17.

The harvested power with external load variation is shown in figure 18. The four units are wired in series and the measured maximum power is 28.5 μW under 43.0 kΩ.

5.2. Power management and supply

AEH array can also be extended. Another four units are mounted adjacent to the previous array and wired in series. To demonstrate power supply ability to a low power electronic device, an electrical power management module EH-300 is utilized, continuously collecting the generated electrical energy packets and accumulating them into a 1000 μF capacitor on board.

At the initial condition, the voltage of the capacitor is zero and the internal voltage needs to build up. When the voltage of the capacitor is higher than 3.5 V, the power management will enable the energy supply, which allows the output voltage to be maintained in a certain range (1.9–3.5 V). In general, the power consumption of the load is larger than the power output from the AEH device, and when the voltage

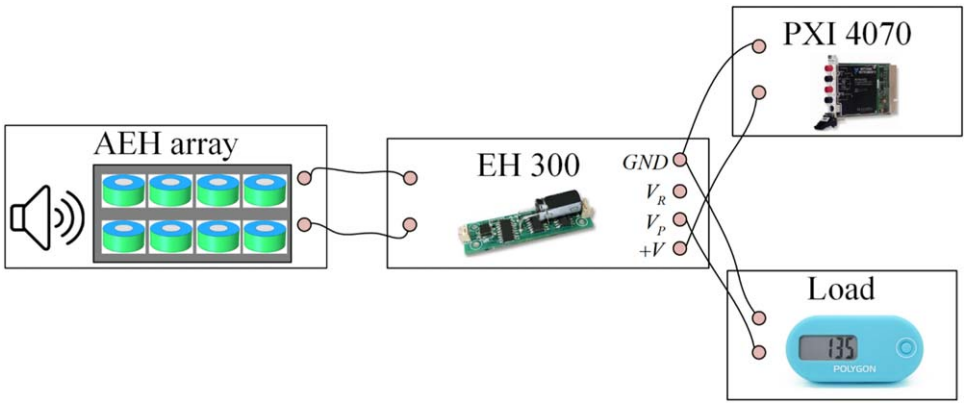

Figure 19. AEH array with the external EH-300 module.

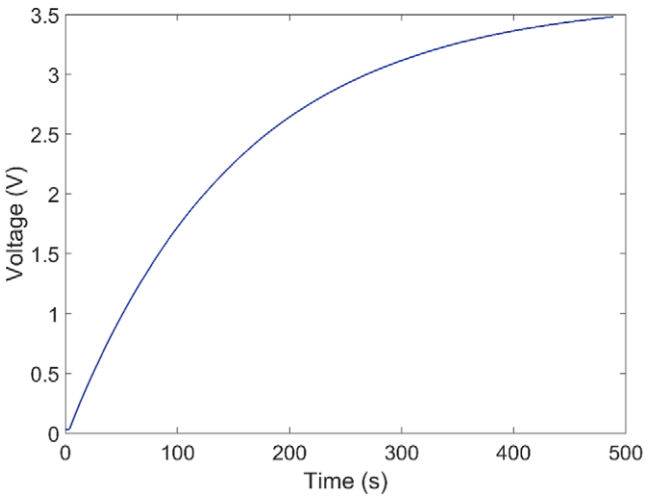

Figure 20. EH-300 charging curve from initial condition to power enable state.

of the capacitor is lower than 1.9 V, the power supply will be closed until the voltage of the capacitor is once again higher than 3.5 V [55].

The schematic diagram of AEH array with the EH-300 module is shown in figure 19. A pedometer (Polygon PD-03) is used as the power consumption target. The internally installed CR2032 cell was removed from the cabin, and electrodes are instead connected to the output terminals of the EH-300 module. Moreover, to observe the charging property, a PXI-4070 module is used to monitor the voltage level.

The recorded charging curve of the EH-300 module from the initial condition to the power enable state is presented in figure 20.

After the power output is enabled, the pedometer can continuously work for approximately 90 s, and then the EH-300 module goes into sleep mode for energy accumulation. Figure 21 shows the working state of the pedometer with the power obtained from the AEH system and the measured SPL level (100.5 dB, without weighting) is demonstrated by a sound level meter (type: AWA-5636).

5.3. Noise reduction performance

The noise reduction performance of the AEH system is investigated and a microphone sensor is adopted to monitor the noise reduction performance. Two cases are compared: one where the waveguide is built by 10 mm acrylic material alone, and the other is where part of the acrylic wall on the top side is replaced by the fabricated AEH array. Figure 22 demonstrates the two working cases.

The excitation signal is band limited white noise (80–200 Hz). Figures 23 and 24 correspondingly show the sound signal comparison in the time domain and in the frequency domain. Under such excitation, the measured SPL is 97.1 dB without the AEH system, and when the AEH system is adopted, the measured SPL reduced to 95 dB. Therefore, 2.1 dB noise reduction is achieved. At some frequencies, the SPL reduction can reach up to 10 dB, indicating that up to 70% noise reduction can be achieved.

Owing to the fact that the energy harvesting capability is not influenced by the noise reduction execution, the proposed system can realize both joint AEH and noise suppression. Meanwhile, the air ventilation function is well retained.

6. Conclusions

In this paper, a deep subwavelength AEH device is proposed, which is designed, verified, and applied from theory to practice. The AEH device contains an embedded spiral neck and a cavity that is able to provide improved sound amplification in the low frequency range. Piezoelectric patch is bonded to the compliant bottom of the cavities, which converts the incident acoustic energy into electrical energy. At 140 Hz, for one AEH unit, 8.1 μW of electrical power can be harvested at the incident SPL of 100 dB.

The proposed AEH device can be extended into array, which is fabricated and mounted on a duct with a sectional area of 306 cm^2. The decoupled property of the AEH unit simplifies the circuit design and the units are linked in series. It is demonstrated that, with the help of a power management module, the AEH array is able to provide electrical power to a pedometer. In further step, more efficient power management

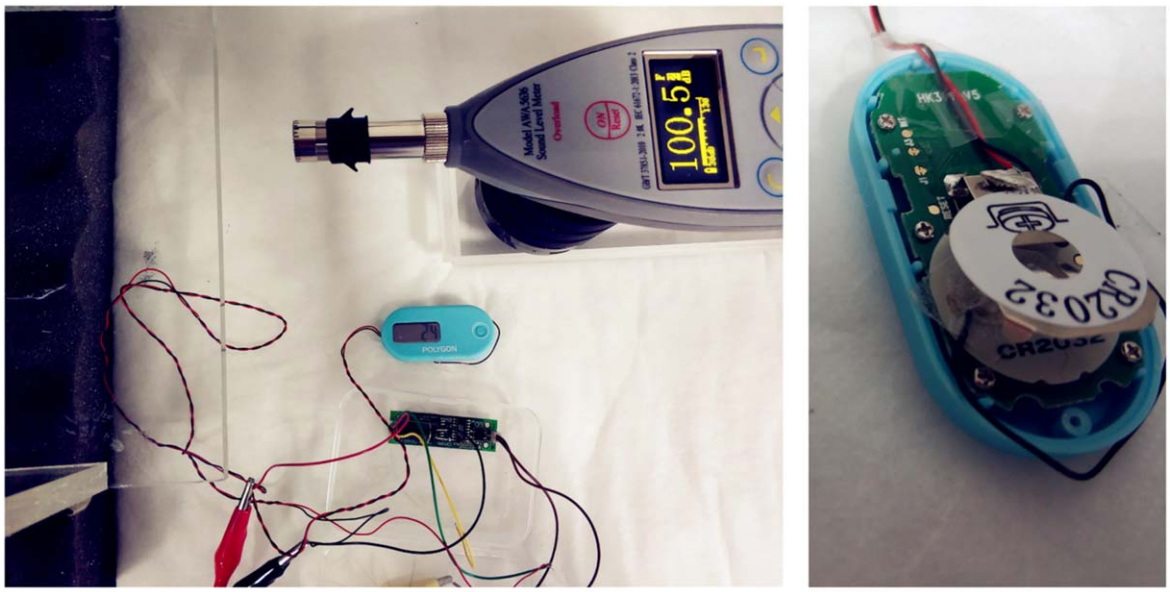

Figure 21. AEH supply electrical power to a pedometer. (a) Pedometer works properly using the harvested acoustic power. (b) Backside view of the pedometer.

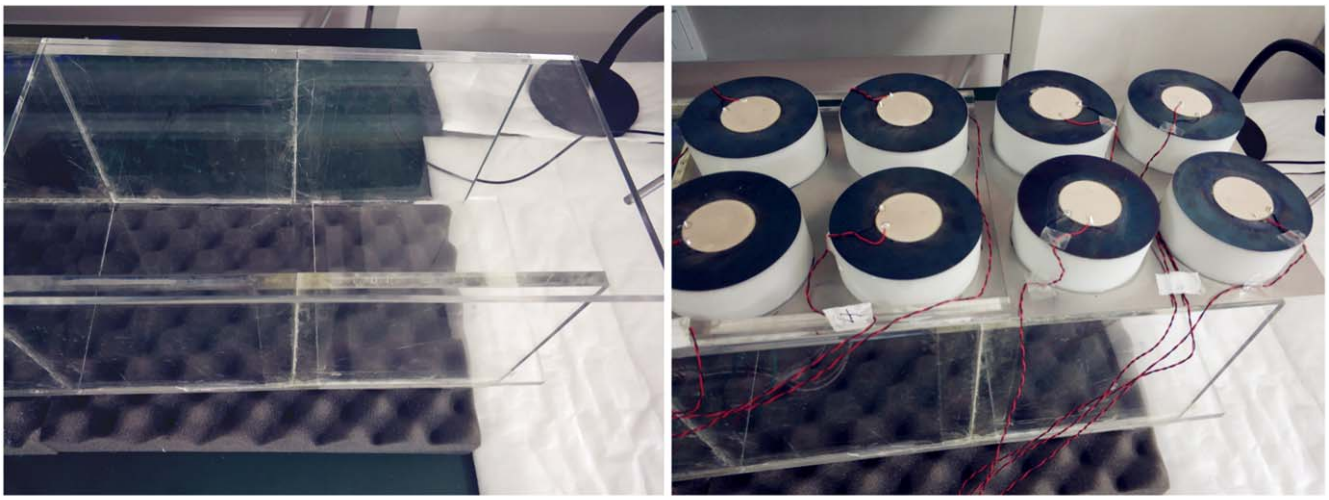

Figure 22. Noise suppression performance of AEH array.

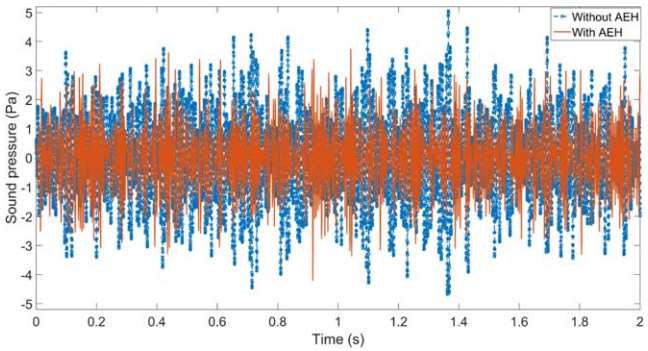

Figure 23. Sound pressure reduction in time domain under 80–200 Hz white noise excitation.

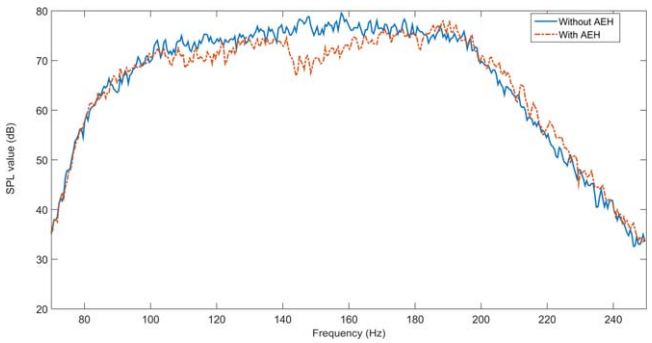

Figure 24. SPL reduction in frequency domain under 80–200 Hz white noise excitation.

scheme will be developed in future studies conducted by the authors.

Meanwhile, the proposed AEH array is able to realize noise reduction. Up to 70% noise can be eliminated when the excitation signal is band limited white noise. In addition, the air ventilation function in the duct is well preserved. For the next procedure, the authors hope to collaborate with industrial partners and deploy the proposed apparatus into suitable places and evaluate its multi-functionalities. This relayed work will be carried out in the near future.

Acknowledgments

The authors sincerely thank the reviewers for their valuable comments and suggestions that have led to the present improved version.

Funding

The present study was supported by the National Natural Science Foundation of China (61701250, 61372044), the Natural Science Foundation of Jiangsu Province (Grant No. BK20160895) and the State Key Laboratory of Mechanical System and Vibration (Grant No. MSV202018).

ORCID iDs

Ming Yuan https://orcid.org/0000-0001-7209-0357
Guoliang Huang https://orcid.org/0000-0003-0959-8427

References

[1] Abdelkareem M A A, Xu L, Ali M K A, Elagouz A, Mi J, Guo S, Liu Y and Zuo L 2018 Vibration energy harvesting in automotive suspension system: a detailed review *Appl. Energy* **229** 672–99
[2] Babayo A A, Anisi M H and Ali I 2017 A review on energy management schemes in energy harvesting wireless sensor networks *Renew. Sustain. Energy Rev.* **76** 1176–84
[3] Ghomian T and Mehraeen S 2019 Survey of energy scavenging for wearable and implantable devices *Energy* **178** 33–49
[4] Yang Z, Zhou S, Zu J and Inman D 2018 High-performance piezoelectric energy harvesters and their applications *Joule* **2** 642–97
[5] Poompavai T and Kowsalya M 2019 Control and energy management strategies applied for solar photovoltaic and wind energy fed water pumping system: a review *Renew. Sustain. Energy Rev.* **107** 108–22
[6] Haras M and Skotnicki T 2018 Thermoelectricity for IoT—a review *Nano Energy* **54** 461–76
[7] Khan F U and Khattak M U 2016 Contributed review: recent developments in acoustic energy harvesting for autonomous wireless sensor nodes applications *Rev. Sci. Instrum.* **87** 021501
[8] Ahmed R, Mir F and Banerjee S 2017 A review on energy harvesting approaches for renewable energies from ambient vibrations and acoustic waves using piezoelectricity *Smart Mater. Struct.* **26** 085031
[9] Choi J, Jung I and Kang C Y 2019 A brief review of sound energy harvesting *Nano Energy* **56** 169–83
[10] Murphy E and King E A 2014 *Transportation Noise Environmental Noise Pollution* ed E Murphy and E A B T-E N P King (Boston: Elsevier) ch 5 pp 123–71
[11] King E A, Pilla F and Mahon J 2012 Assessing noise from wind farm developments in Ireland: a consideration of critical wind speeds and turbine choice *Energy Policy* **41** 548–60
[12] International Standard IEC 61672-1:2002 Electroacoustics—Sound level meters—Part 1: Specifications https://webstore.iec.ch/publication/5708
[13] Crocker M J 2008 *Handbook of Noise and Vibration Control* (New Jersey: Wiley)
[14] Wilby J F 1996 Aircraft interior noise *J. Sound Vib.* **190** 545–64
[15] Barron R F 2002 *Industrial Noise Control and Acoustics* (New York: Marcel Dekker New York)
[16] Bouayed K, Mebarek L, Lanfranchi V, Chazot J D, Marechal R and Hamdi M A 2017 Noise and vibration of a power transformer under an electrical excitation *Appl. Acoust.* **128** 64–70
[17] Wallace C E 1972 Radiation resistance of a rectangular panel *J. Acoust. Soc. Am.* **51** 946–52
[18] Liu F, Phipps A, Horowitz S, Cattafesta L, Nishida T and Sheplak M 2009 Acoustic energy harvesting using an electromechancal Helmholtz resonator *J. Acoust. Soc. Am.* **125** 2596–2596
[19] Peng X, Wen Y, Li P, Yang A and Bai X 2013 A wideband acoustic energy harvester using a three degree-of-freedom architecture *Appl. Phys. Lett.* **103** 1–4
[20] Yang A, Li P, Wen Y, Lu C, Peng X, He W, Zhang J, Wang D and Yang F 2014 Note: high-efficiency broadband acoustic energy harvesting using Helmholtz resonator and dual piezoelectric cantilever beams *Rev. Sci. Instrum.* **85** 066103
[21] Wang Y, Zhu X, Zhang T, Bano S, Pan H, Qi L, Zhang Z and Yuan Y 2018 A renewable low-frequency acoustic energy harvesting noise barrier for high-speed railways using a Helmholtz resonator and a PVDF film *Appl. Energy* **230** 52–61
[22] Khan F and Izhar 2016 Piezoelectric type acoustic energy harvester with a tapered Helmholtz cavity for improved performance *J. Renew. Sustain. Energy* **8** 054701
[23] Horowitz S B, Sheplak M, Cattafesta L N and Nishida T 2006 A MEMS acoustic energy harvester *J. Micromech. Microeng.* **16** 174–81
[24] Yuan M, Cao Z, Luo J, Zhang J and Chang C 2017 An efficient low-frequency acoustic energy harvester *Sensors Actuators* A **264** 84–9
[25] Skow E A, Cunefare K A and Erturk A 2014 Power performance improvements for high pressure ripple energy harvesting *Smart Mater. Struct.* **23** 104011
[26] Lechuga Aranda J J, Bader S and Oelmann B 2019 A space-coiling resonator for improved energy harvesting in fluid power systems *Sensors Actuators* A **291** 58–67
[27] Li B, You J H and Kim Y J 2013 Low frequency acoustic energy harvesting using PZT piezoelectric plates in a straight tube resonator *Smart Mater. Struct.* **22** 055013
[28] Cai X, Guo Q, Hu G and Yang J 2014 Ultrathin low-frequency sound absorbing panels based on coplanar spiral tubes or coplanar Helmholtz resonators *Appl. Phys. Lett.* **105** 1–5
[29] Carrara M, Cacan M R, Toussaint J, Leamy M J, Ruzzene M and Erturk A 2013 Metamaterial-inspired

structures and concepts for elastoacoustic wave energy harvesting *Smart Mater. Struct.* **22** 065004
[30] Chen Z, Guo B, Yang Y and Cheng C 2014 Metamaterials-based enhanced energy harvesting: a review *Physica* B **438** 1–8
[31] Ma F, Wu J H, Huang M, Fu G and Bai C 2014 Cochlear bionic acoustic metamaterials *Appl. Phys. Lett.* **105** 213702
[32] Ma G and Sheng P 2016 Acoustic metamaterials: from local resonances to broad horizons *Sci. Adv.* **2** e1501595
[33] Tan T, Yan Z, Zou H, Ma K, Liu F, Zhao L, Peng Z and Zhang W 2019 Renewable energy harvesting and absorbing via multi-scale metamaterial systems for Internet of things *Appl. Energy* **254** 113717
[34] Assouar B, Liang B, Wu Y, Li Y, Cheng J C and Jing Y 2018 Acoustic metasurfaces *Nat. Rev. Mater.* **3** 460–72
[35] Wang X, Xu J, Ding J, Zhao C and Huang Z 2019 A compact and low-frequency acoustic energy harvester using layered acoustic metamaterials *Smart Mater. Struct.* **28** 025035
[36] Yuan M, Cao Z, Luo J and Pang Z 2018 Helix structure for low frequency acoustic energy harvesting *Rev. Sci. Instrum.* **89** 55002
[37] Nguyen H, Zhu R, Chen J K, Tracy S L and Huang G L 2018 Analytical coupled modeling of a magneto-based acoustic metamaterial harvester *Smart Mater. Struct.* **27** 055010
[38] Sun K H, Kim J E, Kim J and Song K 2017 Sound energy harvesting using a doubly coiled-up acoustic metamaterial cavity *Smart Mater. Struct.* **26** 075011
[39] Qi S and Assouar B 2017 Acoustic energy harvesting based on multilateral metasurfaces *Appl. Phys. Lett.* **111** 243506
[40] Jin M, Liang B, Yang J, Yang J and Cheng J 2019 Ultrathin planar metasurface-based acoustic energy harvester with deep subwavelength thickness and mechanical rigidity *Sci. Rep.* **9** 11152
[41] Monroe N M and Lang J H 2019 Broadband, large scale acoustic energy harvesting via synthesized electrical load: I. Harvester design and model *Smart Mater. Struct.* **28** 55033
[42] Wang Y and Inman D J 2012 A survey of control strategies for simultaneous vibration suppression and energy harvesting via piezoceramics *J. Intell. Mater. Syst. Struct.* **23** 2021–37
[43] Yan B, Zhou S, Zhao C, Wang K and Wu C 2019 Electromagnetic energy harvester for vibration control of space rack: modeling, optimization, and analysis *J. Aerosp. Eng.* **32** 4018126
[44] Tang X and Zuo L 2012 Simultaneous energy harvesting and vibration control of structures with tuned mass dampers *J. Intell. Mater. Syst. Struct.* **23** 2117–27
[45] Hu G, Tang L and Das R 2018 Internally coupled metamaterial beam for simultaneous vibration suppression and low frequency energy harvesting *J. Appl. Phys.* **123** 55107
[46] Ma G, Yang M, Xiao S, Yang Z and Sheng P 2014 Acoustic metasurface with hybrid resonances *Nat. Mater.* **13** 873–8
[47] Li J, Zhou X, Huang G and Hu G 2016 Acoustic metamaterials capable of both sound insulation and energy harvesting *Smart Mater. Struct.* **25** 045013
[48] Zhang X, Zhang H, Chen Z and Wang G 2018 Simultaneous realization of large sound insulation and efficient energy harvesting with acoustic metamaterial *Smart Mater. Struct.* **27** 105018
[49] Mir F, Saadatzi M, Ahmed R U and Banerjee S 2018 Acoustoelastic MetaWall noise barriers for industrial application with simultaneous energy harvesting capability *Appl. Acoust.* **139** 282–92
[50] Mo C, Radziemski L J and Clark W W 2010 Analysis of piezoelectric circular diaphragm energy harvesters for use in a pressure fluctuating system *Smart Mater. Struct.* **19** 1–10
[51] Kim S, Clark W W and Wang Q M 2005 Piezoelectric energy harvesting with a clamped circular plate: analysis *J. Intell. Mater. Syst. Struct.* **16** 847–54
[52] Horowitz S, Nishida T, Cattafesta L and Sheplak M 2002 Characterization of compliant-backplate helmholtz resonators for an electromechanical acoustic liner 40th AIAA *Int. J. Aeroacoustics* **1** 183–205
[53] Nudehi S S, Duncan G S and Farooq U 2013 Modeling and experimental investigation of a helmholtz resonator with a flexible plate *J. Vib. Acoust. Trans. ASME* **135** 041102
[54] Xue Y, Zhao J, Zhang X, Sessler G M and Kupnik M 2019 Acoustic energy harvesting with irradiated cross-linked polypropylene piezoelectret films *Phys. Scr.* **94** 095002
[55] Advanced Linear Devices 2015 Eh300/301 Epad® Energy Harvestingtm Modules 1–4 https://aldinc.com/pdf/EH300.pdf